FISEVIER

#### Contents lists available at ScienceDirect

# **Chemical Geology**

journal homepage: www.elsevier.com/locate/chemgeo



#### Invited research article

# Possible triggers of the seawater sulfate S-isotope increase between 55 and 40 million years ago



Weiqi Yao<sup>a</sup>, Adina Paytan<sup>b,\*</sup>

- <sup>a</sup> Department of Earth Sciences, University of Toronto, Toronto, Ontario M5S 3B1, Canada
- b Institute of Marine Science, University of California-Santa Cruz, Santa Cruz, CA 95064, USA

#### ARTICLE INFO

Keywords:
Sulfur
Sulfate
Sulfur isotopes
Sulfur cycle
Cenozoic
Seawater
Barite
Carbonate associated sulfate
Pyrite

#### ABSTRACT

The Earth system experienced a climatic transition from a greenhouse state to an icehouse state over the Cenozoic, which may have been induced by tectonic and orbital processes. This transition has triggered many environmental changes including fluctuations in sea levels, seawater chemistry, and biogeochemical cycles of carbon, sulfur, and other elements. Owing to a better-resolved biostratigraphic framework and analytical techniques, high temporal resolution seawater sulfate S-isotope data ( $8^{34}S_{sw}$ ) have become available through the analysis of marine barite and carbonate associated sulfate (CAS). These data provide new insight into changes in global biogeochemical cycles over this time interval and their potential causes. This study presents a review of recent work on the  $8^{34}S_{sw}$  for the past 65 million years, with a focus on the most salient perturbation of the Cenozoic sulfur cycle, a 5% rise over a 15-million-year period in the early-middle Eocene. We discuss the possible causes suggested to date for the  $8^{34}S_{sw}$  excursion, which include changes in the magnitude, location, or fractionation associated with pyrite formation and burial, changes to the input of sulfate to the ocean, and changes in ocean circulation. We suggest how some new geochemical data and models can improve our understanding of the various Earth's surface processes that affect the global sulfur cycle and outline a framework for interpreting other geologic intervals where  $8^{34}S_{sw}$  has fluctuated.

#### 1. Introduction

Sulfur is ubiquitous in the Earth's lithosphere, hydrosphere, atmosphere, and biosphere. Sulfur, with an average atomic weight of 32.06, has four stable isotopes 32S, 33S, 34S, and 36S with abundances of approximately 95.02%, 0.75%, 4.21%, and 0.02%, respectively (MacNamara and Thode, 1950; Meija et al., 2016). Due to a broad range of valence states (Table 1), from the fully reduced state (-II) to the fully oxidized state (+VI), sulfur reacts with both metals and non-metal elements. Sulfate is an important oxidant in the present day ocean, predominantly present as dissolved sulfate (SO<sub>4</sub><sup>2-</sup>) in seawater and as sulfate-bearing minerals (e.g., gypsum, barite) in marine sediments. The dissolved sulfate concentration in the ocean at present is ~29 mM (Millero, 2005), and based on the size of the marine sulfate reservoir (approximately  $4 \times 10^{19}$  mol) and sulfate input and output fluxes, the residence time of sulfate in the present-day ocean is on the order of 10 million years (Claypool et al., 1980; Walker, 1986; Jørgensen and Kasten, 2006). Consequently, dissolved sulfate concentrations (normalized to salinity) and the isotopic compositions of sulfate are homogeneously distributed throughout the global open oceans (Rees et al., 1978; Tostevin et al., 2014). However, the concentration of sulfate in seawater and sulfur and oxygen isotopic ratios of dissolved sulfate have changed over Earth's history in response to changes in input/output fluxes of sulfur to/from the ocean and isotopic fractionation associated with chemical transformations of sulfur (e.g., Claypool et al., 1980; Horita et al., 2002; Kampschulte and Strauss, 2004; Paytan et al., 2004; Turchyn and Schrag, 2006; Johnston, 2011; Wu et al., 2015; Rennie et al., 2018).

The biogeochemical cycle of sulfur has been an area of extensive research because changes in the size of the reduced and oxidized reservoirs of sulfur (together with carbon) determine the redox state of the ocean and the level of atmospheric oxygen through time (Berner and Raiswell, 1983; Garrels and Lerman, 1984; Berner, 1989; Petsch and Berner, 1998; Wortmann and Chernyavsky, 2007; Hurtgen, 2012). Transformations between reduced and oxidized sulfur take place primarily in subseafloor anoxic sediments where much of the organic carbon is buried. Under these conditions, sulfate serves as the terminal electron acceptor to remineralize organic matter (OM) through microbial sulfate reduction (MSR:  $2CH_2O + SO_4^{2-} \rightarrow 2HCO_3^{-} + H_2S$ ; Froelich et al., 1979; Jørgensen, 1982; Reeburgh, 1983) and drives

E-mail address: apaytan@ucsc.edu (A. Paytan).

<sup>\*</sup> Corresponding author.

Table 1 Valences of sulfur and representative respective species. Selected species shown are sulfur phases commonly observed in natural environments and laboratory experiments (e.g.,  $S_2O_3^2$  and  $S_3^2$  are important intermediate sulfur compounds associated with microbial sulfate reduction (MSR), Brunner and Bernasconi, 2005; SF<sub>6</sub> is a greenhouse gas and can produce toxic byproducts  $S_2F_2$  and  $S_2F_{10}$ , Dervos and Vassiliou, 2000; SF<sub>6</sub> is also used in S-isotope analyses using the fluorination method; Gao and Thiemens, 1993).

| Valence | -II    | -I       | 0 | I        | II  | III  | IV   | V                        | VI  |
|---------|--------|----------|---|----------|---|--|--|--------------------------|---|
| Species | $H_2S$ | $H_2S_2$ | S | $S_2F_2$ | S <sub>2</sub> O <sub>3</sub> <sup>2-</sup> | HS <sub>2</sub> O <sub>4</sub> <sup>2-</sup> | H <sub>2</sub> SO <sub>3</sub> , SO <sub>3</sub> <sup>2-</sup> | $S_2O_6^{2-}, S_2F_{10}$ | SO <sub>4</sub> <sup>2-</sup> , SF <sub>6</sub> |

anaerobic oxidation of methane (AOM:  $CH_4 + SO_4^{\ 2-} \rightarrow HCO_3^- + HS^- + H_2O$ ; Valentine, 2002; Kasten and Jorgensen, 2000; Jørgensen and Kasten, 2006). These respiration processes are accompanied by large fractionation of sulfur isotopes, leaving the residual seawater sulfate pool enriched in heavy sulfur isotopes. As such, temporal variations in seawater sulfate S-isotope ratios ( $\delta^{34}S_{sw}$ ) can shed light on the nature of changes in the biogeochemical sulfur cycle over geologic time and the processes that control these changes (e.g., Claypool et al., 1980; Paytan et al., 1998; Kampschulte et al., 2001; Kampschulte and Strauss, 2004; Paytan et al., 2004; Bottrell and Newton, 2006; Rennie et al., 2018; Yao et al., 2018; Toyama et al., 2020).

Over the past decades, scientists have utilized various archives for reconstructing  $8^{34}S_{sw}$  over the Cenozoic (Claypool et al., 1980; Paytan et al., 1998; Paytan et al., 2004; Turchyn et al., 2009; Markovic et al., 2015; Markovic et al., 2016; Masterson et al., 2016; Rennie et al., 2018; Yao et al., 2018; Toyama et al., 2020; Yao et al., 2020; Toyama et al., 2020). Although these relatively high temporal resolution data from multiple sites have constrained the changes in  $\delta^{34}S_{sw}$  over the Cenozoic, the underlying drivers that cause these changes remain controversial. This review summarizes the currently available high-resolution  $\delta^{34}S_{sw}$  data for the Cenozoic, presents the various forcing mechanisms put forth to explain the secular variations in  $\delta^{34}S_{sw}$ , and suggests some future research needs that could better constrain possible interpretations.

## 2. The global sulfur cycle

The concentration of sulfate in seawater and  $\delta^{34}S_{sw}$  are controlled by the riverine and volcanic sulfur input to the ocean and the sulfur output via burial of sulfur-bearing minerals and their respective S-isotope signatures (Fig. 1). Terrestrial weathering and transport of dissolved sulfur species to the ocean constitutes the dominant sulfur source. Tectonic uplift and sea-level changes expose buried minerals to oxidative weathering environments, where pyrite oxidation and evaporite dissolution contributes about  $1.5 \times 10^{12}$  to  $3.5 \times 10^{12}$  mol sulfur per year to seawater via river runoff (Holland, 1974; Meybeck, 1979; Garrels and Lerman, 1984; Kump and Garrels, 1986; Canfield, 2004; Calmels et al., 2007; Tostevin et al., 2014; Burke et al., 2018). Since sulfate-bearing evaporites (e.g., gypsum, anhydrite) precipitate

with little or no S-isotope fractionation from coeval seawater sulfate, weathering and precipitation of evaporites usually exert minor influence on  $\delta^{34}S_{sw}$  (Claypool et al., 1980, but see Wortmann and Chernyavsky, 2007; Wortmann and Paytan, 2012). Conversely, sedimentary pyrite inherits the 34S-depleted signature of sulfide produced by MSR where fractionation between sulfate and sulfide can be as high as 72% (Kaplan et al., 1963; Strauss, 1997; Rudnicki et al., 2001; Wortmann et al., 2001; Canfield et al., 2010; Wu et al., 2010). Thus, pyrite burial plays a key role in governing  $\delta^{34}S_{sw}$  (e.g., Berner and Raiswell, 1983; Garrels and Lerman, 1984; Walker, 1986; Berner and Berner, 1987; Berner, 1989; Petsch and Berner, 1998). The estimated annual burial of pyrite and evaporite removes  $1.5 \times 10^{12}$  to  $4.3 \times 10^{12}$  mol sulfur per year, respectively, from the ocean (Garrels and Lerman, 1984; Kump and Garrels, 1986; Walker, 1986; Tostevin et al., 2014; but see Halevy et al., 2012). In addition, volcanic and hydrothermal activities transfer  $0.2 \times 10^{12}$  to  $1.5 \times 10^{12}$  mol sulfur per year to seawater with  $\delta^{34}$ S values of 0% to 5% (Ohmoto and Rye, 1979; Sakai et al., 1982; Walker, 1986; Stoiber et al., 1987; Eldholm and Thomas, 1993; Hansen and Wallman, 2003; Canfield, 2004).

Assuming the sulfur cycle is in mass and isotopic steady state, the flux and isotopic ratio of sulfur delivered into the ocean should equal the flux and isotopic ratio of the total sulfur sink as pyrite and evaporite burial (Eqs. (1) and (2)):

$$F_{in} = F_{out} = F_{evaporite} + F_{pyrite}$$
 (1)

$$F_{in} \cdot \delta^{34} S_{in} = F_{evaporite} \cdot \delta^{34} S_{sw} + F_{pyrite} \cdot \delta^{34} S_{pyrite}$$
(2)

This can also be expressed as the time-dependent seawater sulfate concentration and  $\delta^{34}S_{\text{\tiny SW}}$ :

$$dM_{sw}/dt = F_{in} - F_{evaporite} - F_{pyrite}$$
(3)

$$d(M_{sw}\cdot\delta^{34}S_{sw})/dt = F_{in}\cdot\delta^{34}S_{in} - F_{evaporite}\cdot\delta^{34}S_{sw} - F_{pyrite}\cdot(\delta^{34}S_{sw} - \Delta)$$
 (4)

where  $M_{sw}$  is the concentration of seawater sulfate;  $F_{in}$  is the total influx of sulfur to the ocean, with contributions from evaporite dissolution, oxidative weathering of sedimentary and igneous sulfide minerals, and volcanic degassing of sulfur volatiles;  $\delta^{34}S_{in}$  is the S-isotope ratio of this influx, which depends on the relative contributions of these three components;  $F_{evaporite}$  and  $F_{pyrite}$  are the burial fluxes of sulfate as

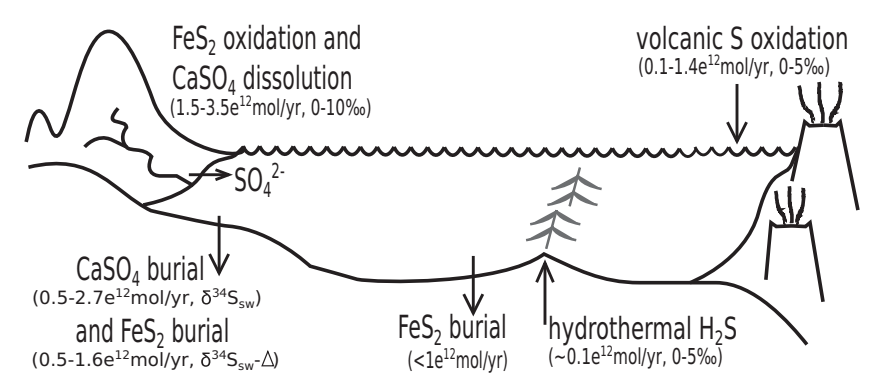


Fig. 1. Simplified sketch of global sulfur cycling in the present-day ocean. References for the concentrations and fluxes depicted in the figure are provided in the text above.

evaporites and pyrite, respectively;  $\delta^{34}S_{sw}$  is the S-isotope ratio of seawater sulfate;  $\Delta$  is the average difference (in permil) between the δ<sup>34</sup>S values of contemporaneous seawater sulfate and the pyrite sedimentary sink. Notably, the only parameters that can be directly and accurately obtained for the geological past are the  $\delta^{34}S_{sw}$  value (as measured in sulfate minerals from marine sediments, e.g., evaporites, barite, carbonate associated sulfate) and the rate of change in  $\delta^{34}S_{\text{sw}}$ (i.e.,  $d\delta^{34}S_{sw}/dt$ ) if the ages of the analyzed samples are well constrained and the temporal resolution of the samples is sufficient to define the rate of change. All other parameters are either derived from low-resolution datasets (e.g., fluid inclusions for Msw; Horita et al., 2002), from laboratory experiments (e.g., Δ; Sim et al., 2011; Wing and Haleyy, 2014), or assumed based on knowledge of the present-day sulfur cycle and the geological, geochemical, and biological processes that control it (e.g., spreading rate, volcanic activity, shelf area, weathering rate and exposure of weathered rocks; Holser et al., 1988; Canfield, 2004; Paytan et al., 2004; Halevy et al., 2012; Markovic et al., 2015; Burke et al., 2018). As a result, multiple solutions to the mass balance equations are possible, and several solutions can explain the prominent fluctuations in the secular  $\delta^{34}S_{\rm sw}$  as emphasized in Paytan et al. (2004). Here we focus on the Cenozoic record and the various interpretations that have been proposed to explain the fluctuation in δ<sup>34</sup>S<sub>sw</sub> over this time interval, as it represents a period for which the available data are of high fidelity and temporal resolution.

# 3. The Cenozoic $\delta^{34}S_{sw}$ record of seawater sulfate

The Cenozoic  $\delta^{34}S_{sw}$  has been reconstructed using marine evaporites, carbonate associated sulfate (CAS), and marine pelagic barite as archives. The evaporite-based  $\delta^{34}S_{sw}$  data initially presented by Claypool et al. (1980) with further work (Utrilla et al., 1992; Strauss et al., 2001; Kampschulte and Strauss, 2004; Orti et al., 2010) reveal fluctuations in  $\delta^{34}S_{sw}$  during the Cenozoic. However, due to the intermittent occurrence of evaporites and a scarcity of microfossils in evaporitic basins, these records are often plagued by large age uncertainties. Marine pelagic barite and CAS often provide more continuous and robust records with better constraints on age (e.g., Paytan et al., 1998; Turchyn et al., 2009; Rennie et al., 2018; Yao et al., 2018; Toyama et al., 2020; Yao et al., 2020). The current CAS and barite derived  $\delta^{34}S_{sw}$  records for the Cenozoic have a temporal resolution of < 1 million years with data spread of approximately 0.2% within each time interval (Yao et al., 2019 and references therein).

Here we present a compilation of  $\delta^{34}S_{sw}$  data derived from CAS and pelagic barite sampled from deep-sea sediments from worldwide locations (Fig. 2; Paytan et al., 1998; Turchyn et al., 2009; Markovic et al., 2015; Markovic et al., 2016; Masterson et al., 2016; Rennie et al., 2018; Yao et al., 2018; Toyama et al., 2020; Yao et al., 2020). We recalculate the ages of these samples in accordance with the GTS2012 timescale (Gradstein et al., 2012) using the Neptune database (Lazarus, 1994; Spencer-Cervato, 1999). This database provides an extensive review of microfossil occurrence records from Deep Sea Drilling Project (DSDP), Ocean Drilling Program (ODP), and Integrated Ocean Drilling Program (IODP) publications for each core and converts biostratigraphic zones into absolute ages.

The  $\delta^{34}S_{sw}$  over the past 65 million years varies between 16‰ and 24‰ (Fig. 2). The  $\delta^{34}S_{sw}$  value decreases from  $\sim\!19\%$  to  $\sim\!17\%$  between 65 and  $\sim\!55$  Ma. Following this minimum, the  $\delta^{34}S_{sw}$  value shows a pronounced positive 5‰ shift to  $\sim\!22.5\%$  at 40 Ma. The gradient of the increase is approximately 0.4‰/Myr. From 40 Ma until  $\sim\!3$  Ma the  $\delta^{34}S_{sw}$  value stays relatively constant, and during the last 3 million years, the  $\delta^{34}S_{sw}$  value declines by  $\sim\!1\%$  to the present-day value of 21‰. Data from different ocean basins exhibit a good agreement on the overall shape, timing, and magnitude of the excursion (see Supplementary file), indicating that such variations in  $\delta^{34}S_{sw}$  are primary and, most importantly, global.

The  $\delta^{34}S_{sw}$  record shows a clear offset between the CAS and barite

data for each time interval. To estimate the  $\delta^{34}S_{sw}$  value at any given time, we use a "local regression smoothing" module (LOESS; Cleveland, 1979) in the statistical software package R (R Core Team, 2012) for each respective data set. The "span" value for the regression is 0.5. We calculate the 95% confidence interval for each datum point from the standard errors returned by the LOESS function.

Our results demonstrate that the compiled CAS (blue) and marine barite (red) derived  $\delta^{34} S_{sw}$  records track each other with high fidelity (Fig. 3). However, an offset of up to 1% exists between the two data sets. This points to either 1) effects of using different analytical methods, 2) effects of diagenetic alteration on one or both of the records, or 3) S-isotope fractionation during precipitation of one or both minerals. Most of the studies use isotope ratio mass spectrometry (IRMS) for the  $\delta^{34}S_{sw}$  analyses, where sulfate in the solid phase is converted to sulfur hexafluoride (SF<sub>6</sub>) in an offline mode (e.g., Paytan et al., 1998; Masterson et al., 2016) or to sulfur dioxide (SO2) in a continuous-flow mode (e.g., Turchyn et al., 2009; Toyama et al., 2020; Yao et al., 2020). The single-species foraminifera samples reported by Rennie et al., (2018) are analyzed by a recently developed multi-collector inductively coupled plasma mass spectrometry (MC-ICP-MS) method for CAS analyses, which allows measurements of samples of just a few nmol sulfur (Paris et al., 2013; Paris et al., 2014). The analytical accuracy of all of the above methods is approaching 0.1% (Grassineau et al., 2001; Paris et al., 2013; Paris et al., 2014; Yao et al., 2020) and all laboratories report data relative to the Vienna Cañon Diablo Troilite (VCDT) standard using international reference materials (e.g., IAEA-SO-5 (0.49%), NBS 127 (21.12%); Coplen et al., 2001), so the offset between records is unlikely due to the use of different analytical procedures.

Positive S-isotope offsets from contemporaneous seawater can be due to diagenetic overprinting. In sediments where microbial sulfate reduction occurs, the residual porewater sulfate becomes enriched in <sup>34</sup>S relative to contemporaneous seawater sulfate and can be incorporated into carbonate or barite that forms diagenetically post burial. Under such reducing conditions, carbonate and even barite (which is resistant to diagenesis as long as the interstitial water is saturated with respect to barium sulfate) are prone to dissolution and recrystallization (Dymond et al., 1992; Torres et al., 1996; Paytan et al., 2002; Kampschulte and Strauss, 2004; Rennie and Turchyn, 2014). However, mineral morphology, porewater geochemistry (e.g., sulfate concentrations, organic matter and pyrite contents, sedimentation rates) of the cores, and the foraminiferal tests used in Fig. 2 have been carefully examined to avoid diagenetically recrystallized samples (e.g., Paytan et al., 2002; Rennie et al., 2018; Toyama et al., 2020; Yao et al., 2020). Moreover, diagenesis depends on local conditions in the porewater and hence is unlikely to exert a constant effect on CAS and barite  $\delta^{34}S_{sw}$  across a variety of locations and for 65 million years back in time.

Recent studies suggest that the offset between CAS and barite  $\delta^{34}S_{sw}$ values can be a consequence of S-isotope fractionation during biomineralization (Rennie et al., 2018; Toyama et al., 2020). Toyama et al. (2020) report the S-isotope compositions of CAS and marine barite of the same age from the same cores (i.e., IODP Site U1331 and U1333). The observed CAS  $\delta^{34}S_{sw}$  values are consistently 0.5% to 1.1% higher than the coexisting barite  $\delta^{34}S_{sw}$  with no temporal change in the magnitude of the offset. This suggests that the original signals are retained in both phases. Indeed, the formation of CAS involves speciesspecific S-isotope fractionation of up to  $\pm$  1% from the coeval seawater sulfate (Kampschulte and Strauss, 2004; Paris et al., 2014) and between different foraminiferal species (Rennie et al., 2018), which may account for the constant offset in Fig. 3. Therefore, correction for vital effects is required in future studies by utilizing single-species foraminifera for CAS  $\delta^{34}S_{sw}$  analyses and/or through direct comparisons between CAS and barite  $\delta^{34}S_{sw}$  from the same sample.

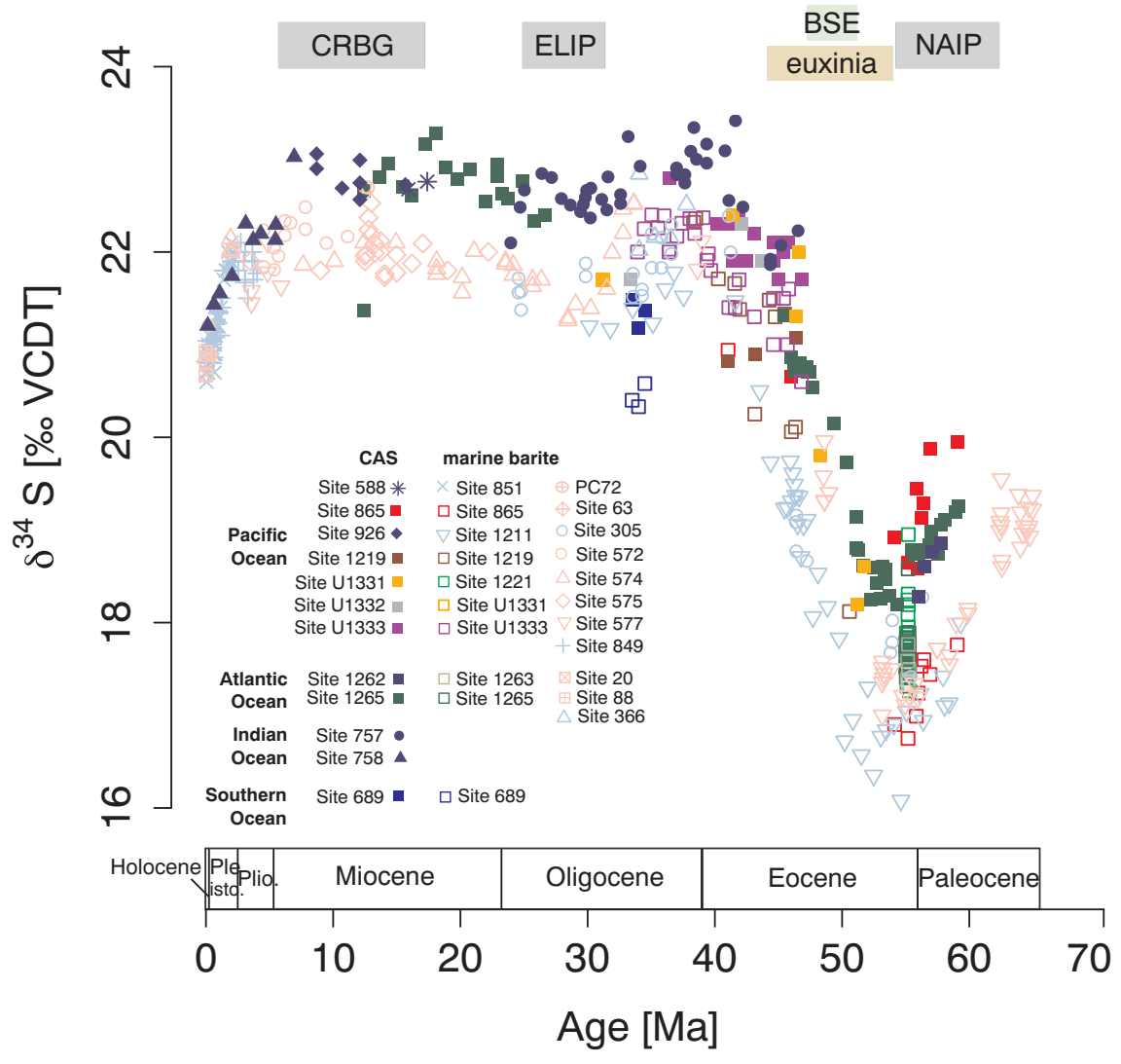


Fig. 2. The  $\delta^{34}S_{sw}$  record for the Cenozoic. Analytical errors range between 0.1% and 0.3% (1 $\sigma$ ; see Supplementary data). All the data are mapped on the GTS2012 timescale (Lazarus, 1994; Spencer-Cervato, 1999; Gradstein et al., 2012). Major geologic events are highlighted on the top, including major magmatic events (CRFB = Columbia River Flood Basalt at 17–6 Ma,  $1.75 \times 10^5$  km³; ELIP = Ethiopian Large Igneous Province at 31–25 Ma,  $3.5 \times 10^5$  km³; NAIP = North Atlantic Igneous Province at 62–55 Ma,  $6.6 \times 10^6$  km³; Ross et al., 2005), basin-scale evaporite (BSE) dissolution events at 51–47 Ma (1.97  $\times 10^{19}$  mol CaSO<sub>4</sub>; Wortmann and Paytan, 2012), and potential oceanic euxinia in the isolated Arctic basin at 54–44 Ma (Kurtz et al., 2003; Ogawa et al., 2009; Toyama et al., 2020). Note that we exclude the DSDP Site 366 data for the mid-Eocene and lower sections (> 38 Ma), where the samples have undergone diagenetic alteration (Yao et al., 2020). Marine pelagic barite data from Paytan et al., 1998, Turchyn et al., 2009, Markovic et al., 2015, Markovic et al., 2016, Masterson et al., 2016, Yao et al., 2018, Toyama et al., 2020, Yao et al., 2020; CAS data from Turchyn et al., 2009, Rennie et al., 2018, Toyama et al., 2020.

## 4. Potential mechanisms for the 5% rise in the early Cenozoic

The most pronounced perturbation of the Cenozoic sulfur record is the 5% rise in  $\delta^{34}S_{sw}$  over an approximately 15-Myr period in the early to middle Eocene (Fig. 2). Existing explanations for the cause of the +5%  $\delta^{34}S_{sw}$  shift include a) a change in the dominant locus of pyrite burial and the associated pyrite S-isotope composition ( $\delta^{34}S_{pyrite}$ ) corresponding to sea-level and tectonic changes (Rennie et al., 2018), b) extensive pyrite burial under euxinic conditions in epicontinental seas (Kurtz et al., 2003) or in the Arctic Ocean (Ogawa et al., 2009; Toyama et al., 2020), c) increased pyrite burial rates as a result of increasing seawater sulfate concentrations associated with punctuated sulfur inputs from basin-scale evaporite dissolution (Wortmann and Paytan, 2012) or Large Igneous Provinces (PI; Laakso et al., 2020). Alternative trigger mechanisms, based on recent interpretations of sulfur cycle evolution derived from novel approaches (e.g., Halevy et al., 2012; Canfield, 2013; Tostevin et al., 2014; Burke et al., 2018), are also possible.

## 4.1. Sea-level variations and pyrite burial

It is traditionally assumed that with abundant sulfate in seawater, microbial sulfate reduction (MSR) rates and the dominant pathway of sulfide reoxidation depend chiefly on the availability of organic matter (OM) and microbial activity (Goldhaber and Kaplan, 1975; Berner, 1982; Jørgensen, 1982; Berner and Raiswell, 1983; Jørgensen, 1987; Thamdrup et al., 1994; Jørgensen and Nelson, 2004). In areas where sedimentation rates are fast, OM concentrations are high, and OM degradation can readily deplete oxygen (as well as dissolved nitrate, iron, and manganese) in the interstitial water, allowing for the occurrence of MSR and pyrite burial (Goldhaber and Kaplan, 1975; Berner, 1982; Jørgensen, 1982). Consequently, burial rates of OM and pyrite sulfur appear to be positively correlated in modern marine sediments (Berner, 1982; Berner and Raiswell, 1983; Raiswell and Berner, 1985). Continental shelves are characterized by high sedimentation rates and high productivity and are thus loci of pyrite burial. When sea-level is low, pyrite in the exposed continental shelves will be subjected to oxidative

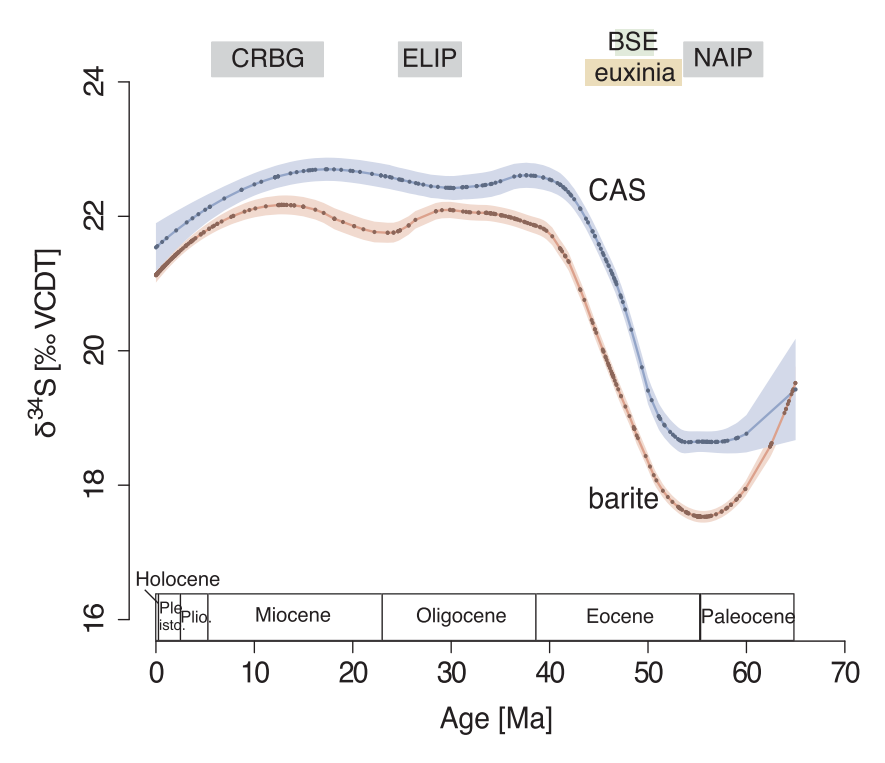


Fig. 3. The LOESS curves for the marine barite and CAS derived  $8^{34}S_{sw}$  records for the last 65 million years. The red and the blue envelopes denote the 95% confidence intervals of the LOESS regressions for the barite and CAS data, respectively. The relatively large uncertainty for the CAS curve between 65 and 60 Ma is likely due to the low resolution of the data. Both curves are mapped on the GTS2012 timescale (Lazarus, 1994; Spencer-Cervato, 1999; Gradstein et al., 2012). Note that the LOESS curves smooth out finer fluctuations that may be present, which may lead to bias in determining isotopic values and age resolution. Major geologic events are highlighted on the top (see Fig. 2 caption for details). (For interpretation of the references to color in this figure legend, the reader is referred to the web version of this article.)

weathering (Turchyn and Schrag, 2006; Markovic et al., 2015; Kölling et al., 2019). Hence, both pyrite weathering and pyrite burial are sensitive to the size of continental shelves. During sea-level high stands, shelf areas expand, and pyrite burial becomes more prevalent, whereas during sea-level low stands, shelf areas shrink, and the previously buried pyrite is reoxidized.

However, the marine sulfur and carbon isotopic records indicate the decoupling of OM and pyrite burial over the Cenozoic (Paytan et al., 1998; Zachos et al., 2001; Kurtz et al., 2003; Rennie et al., 2018). One possibility to reconcile this observation is spatial decoupling in which the location of pyrite burial changes without substantial changes in the pyrite burial flux (Rennie et al., 2018). Due to tectonic reorganization and a rapid sea-level decline in the early Eocene (Golonka, 2004; Bouilhol et al., 2013; Miller et al., 2005), the loss of epicontinental seas and shallow shelves drives the depositional depth of pyrite from shallow to deep waters. Subaerial exposure of previously submerged shallow sedimentary basins enhances carbon and iron delivery to the ocean, resulting in an increase in pyrite burial in the deeper ocean at the expense of burial at shallower depths (i.e., shelves and epicontinental seas). Based on the assumption of a larger fractionation of pyrite burial and hence a more negative  $\delta^{34}S_{pvrite}$  in the deep ocean relative to nearshore environments (Fike et al., 2015), the global average S-isotope difference between seawater sulfate and pyrite has to increase from approximately -30% to -41% in the early Eocene and stay at around -41% for the remainder of the Cenozoic (Rennie et al., 2018). These combined changes (in the location of pyrite burial and  $\delta^{34}S_{pyrite}$ ) may have been the cause for the irreversible 5% rise in  $\delta^{34}S_{sw}$ .

While the above scenario provides a possible explanation, it is currently not clear why  $\delta^{34}S_{pyrite}$  values will be different in different marine sedimentary settings (Kaplan et al., 1963; Strauss, 1997; Fike et al., 2015). In particular, a decrease in  $\delta^{34}S_{pyrite}$  value (hence an increase in  $\delta^{34}S_{sw}$ ) during lower sea-level periods seems to be incompatible to the -1% shift in  $\delta^{34}S_{sw}$  during the Quaternary (Markovic et al., 2015; Rennie et al., 2018), where a comparable magnitude of sea-level decline is demonstrated (Miller et al., 2005). Direct evidence for the influence of changing deposition areas and relevant redox conditions, and isotope fractionation associated with microbial ecology, MSR and sulfide reoxidation, and pyrite formation is

further required. This evidence can be obtained in experimental tests representing the natural environments or via observations at different oceanic settings today. Moreover, the relationship between minor sulfur isotopes ( $^{33}$ S and  $^{36}$ S) and  $^{34}$ S within the range of mass-dependent fractionation can be an additional tool to identify different metabolic processes and to shed light on the underlying environmental information (Farquhar and Wing, 2003; Johnston et al., 2005; Johnston et al., 2008; Zerkle et al., 2009; Zerkle et al., 2010; Johnston, 2011; Sim et al., 2011; Wing and Halevy, 2014; Kunzmann et al., 2017).

The oxygen isotopic record of seawater sulfate ( $\delta^{18}O_{sw}$ ) can also trace the effect of sea-level variations on sulfur cycling (Turchyn and Schrag, 2006; Markovic et al., 2016). Abiotic sulfide oxidation is dominant in abyssal oxic sediments, whereas microbial sulfur disproportionation and microbial sulfide oxidation are more favorable in low-oxygen sediments on continental shelves (Jørgensen et al., 1991; Zopfi et al., 2001; Turchyn and Schrag, 2006; Markovic et al., 2016). Since different pathways impart distinct fractionations of oxygen isotopes in sulfate (Van Stempvoort and Krouse, 1994; Böttcher and Thamdrup, 2001; Böttcher et al., 2001; Böttcher et al., 2005; Balci et al., 2012; Antler et al., 2013; Antler et al., 2017), interpreting  $\delta^{18}O_{sw}$  (together with  $\delta^{34}S_{sw}$ ) records may provide additional constraints on the possibility of the above changes in burial loci and  $\delta^{34}S_{pvrite}$  scenario.

#### 4.2. Pyrite burial in euxinic environments

Pyrite can precipitate directly in the water column under euxinic (i.e., anoxic and sulfidic) conditions (Raiswell and Berner, 1985; Rickard, 2012). In normal marine environments where bottom water is well oxygenated (Fig. 4A), the organic carbon to pyrite sulfur ( $C_{\rm org}/S_{\rm py}$ ) ratio is approximately 2.8 on a weight basis (i.e., a molar ratio of 7.5; Berner and Raiswell, 1983). In euxinic environments, MSR occurs both in sediments and in the water column, resulting in excess dissolved H<sub>2</sub>S and the subsequent pyrite formation directly from seawater (Fig. 4B). The  $C_{\rm org}/S_{\rm py}$  ratio under euxinic conditions is lower than 2.8 (Berner and Raiswell, 1983). Hence, the  $C_{\rm org}/S_{\rm py}$  ratio can serve as an indicator of different marine environments. Moreover, a lower  $C_{\rm org}/S_{\rm py}$  ratio would imply that for each carbon available as a substrate, potentially more pyrite is buried, removing more  $^{32}S$  and thus inducing an increase

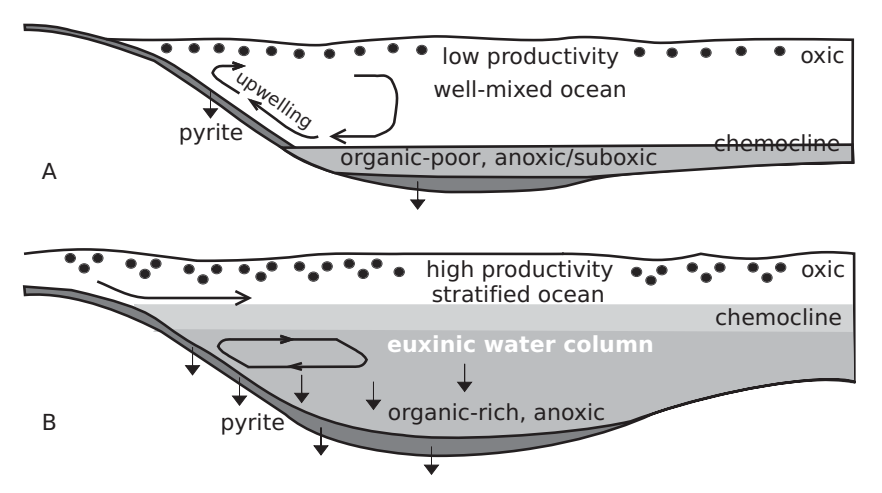


**Fig. 4.** Schematic diagram of the development of marine euxinic conditions. (A) Normal marine environment: pyrite precipitates in anoxic sediments in the zone of microbial sulfate reduction,  $C_{\rm org}/S_{\rm py} \approx 2.8$  (Berner and Raiswell, 1983). (B) Euxinic environment in a stratified ocean: pyrite formation takes place both in the sulfidic water column and in euxinic sediments,  $C_{\rm org}/S_{\rm py} < 2.8$  (Raiswell and Berner, 1985; Meyer and Kump, 2008).

in the residual sulfate  $\delta^{34}S$ .

Kurtz et al. (2003) attribute the rapid rise in  $\delta^{34}S_{sw}$  to a pulse of pyrite burial in widespread euxinic environments along inland seas and continental shelves in the early Eocene. They suggest that the rise in δ<sup>34</sup>S<sub>sw</sub> coincides with a period of low organic carbon burial and a decline in  $C_{\rm org}/S_{\rm py}$  burial in response to an increase in euxinic marine environments. This in turn will increase  $\delta^{34}S_{sw}$ . However, applying this modeling approach to the current high-resolution updated  $\delta^{34}S_{sw}$  data, the excursion spans a broader period than originally reported (~55-40 Ma in this study compared to 56-47 Ma in Paytan et al. (1998)). This adjustment shifts the timing of the  $\delta^{34}S_{sw}$  rise towards the middle Eocene, a time that is characterized by a long-term trend of falling sea level, rather than being confined to the early Eocene marine transgression (Miller et al., 2005). In other words, the maximum in pyrite burial may no longer coincide with a minimum in organic carbon burial and a low  $C_{\rm org}/S_{\rm py}$  ratio. Rather, the  $C_{\rm org}/S_{\rm py}$  ratio may be more in line with normal marine environments in the early and middle Eocene. Additional observations of Corg/Spy ratios in various locations and more modeling tests are required to reevaluate the timing and extent of ocean euxinia.

Another concern for this hypothesis is a lack of evidence for an increase in sedimentary pyrite burial rates in marine sediments of the appropriate age. Geological records for high pyrite burial in the early and middle Eocene are only reported for the Arctic basin (Newell, 2001; Stein et al., 2006; Ogawa et al., 2008; Dickson and Cohen, 2012).

#### 4.3. Pyrite burial in the Arctic Ocean

Ogawa et al. (2008) report an average total sulfur (%TS) of  $\sim$ 6.7% (ranged from 2.6% to 19.4%) in sediments of early-middle Eocene age on the Lomonosov Ridge in the central Arctic. This value is substantially higher than seen in Mediterranean sapropels ( $\leq$ 2%), modern Black Sea (euxinic) sediments ( $\sim$ 2%), and in Cretaceous black shales (up to 6%; Brumsack, 1980; Berner, 1982; Böttcher et al., 2003). Taking sediment mass accumulation rates into account, the coeval total sulfur accumulation rate reaches as high as 1 g cm $^{-2}$  kyr $^{-1}$  (Ogawa et al., 2008). The presence of framboidal pyrite as the main sulfur form and the low  $C_{org}/S_{py}$  ratio for the early and middle Eocene intervals in these sediments support the idea that intensive MSR has occurred under euxinic bottom water environment in the Arctic Ocean (Berner, 1970; Kohn et al., 1998; Ogawa et al., 2008). The S-isotope ratio of this pyrite is on average approximately -40% and can be more depleted, reaching a value of -58.5% (Ogawa et al., 2008).

The idea of extensive pyrite burial in the Eocene Arctic basin is intriguing because of its unique paleogeographic and paleoceanographic features. The Arctic has been nearly disconnected from the other ocean basins in the early-middle Eocene (Fig. 5A), and seawater is

exchanged via "estuarine circulation" developing strong salinity stratification in the surface waters (Berger, 1970; Akhmetiev and Beniamovski, 2004). Unlike the modern euxinic Black Sea where iron input is limited (Lyons and Berner, 1992), the "estuarine circulation" pattern allows sufficient nutrients and iron input from river runoffs into the Arctic basin (Fig. 5B; Ogawa et al., 2008). This mechanism enables OM production and accumulation and the consequent anoxic condition in the bottom water, supporting the continuous formation of pyrite. When tectonic processes facilitate the connection between the Arctic Ocean and the North Atlantic (Akhmetiev and Beniamovski, 2004), the  $^{34}\mathrm{S}\text{-enriched}$  Arctic seawater mix with the rest of the world oceans, leading to a global increase in  $\delta^{34}\mathrm{S}\text{-sw}$ . Subsequently, the local euxinia in the Arctic Ocean ceases.

Using the present-day seawater sulfate concentration of 29 mM (Millero, 2005), Ogawa et al. (2008) estimate a local deposition of approximately 7  $\times$   $10^{13}$  tons sulfur in the euxinic Arctic basin between 54 and 44 Ma. They conclude that this amount of reduced sulfur burial can explain a 3‰ rise in the global  $\delta^{34}S_{sw}$  at that time. If the concentration of sulfate in seawater during the Eocene is lower as some evidence suggests (~14 mM; Horita et al., 2002; Halevy et al., 2012), the discharge of this  $^{34}S$ -enriched Arctic seawater to the global oceans may explain the entire 5‰ increase (Toyama et al., 2020). In addition, the revised  $\delta^{34}S_{sw}$  rise towards younger ages (55–40 Ma) now agrees better with the documented time interval (~44 Ma) of pyrite burial in the Arctic basin.

#### 4.4. Tectonic uplift and basin-scale evaporite dissolution

On geologic timescales, the sulfur cycle responds to changes in the relative proportion of sulfate and sulfide input and output to and from the ocean. Tectonic processes uplift buried sediments into terrestrial environments where sulfur-bearing minerals undergo weathering releasing sulfate. Unlike pyrite that is insoluble without exposure to oxidants (e.g., O<sub>2</sub>, Fe<sup>3+</sup>; Moses et al., 1987), sulfate-bearing evaporite minerals are very soluble and can readily release sulfate into solution.

Wortmann and Paytan (2012) interpret the  $\delta^{34}S_{sw}$  rise as evidence for an increase in pyrite burial caused by an increase in marine sulfate concentrations in the early Eocene. They suggest that the initial collision between India and Eurasia may have intensified basin-scale evaporite dissolution, releasing approximately  $2\times 10^{19}$  mol of CaSO<sub>4</sub> from continents to the ocean between 51 and 47 Ma (Wortmann and Paytan, 2012). Because the seawater sulfate concentration in the early-Cenozoic is low (Horita et al., 2002), this dissolution event can effectively increase  $\delta^{34}S_{sw}$  for two reasons. First, the sulfate released from Neoproterozoic to Early Cambrian evaporite deposits along the Paleotethys margins (Zharkov, 1981) is characterized by high  $\delta^{34}S_{sw}$  values relative to the early Eocene seawater sulfate (Claypool et al., 1980; Yao et al.,

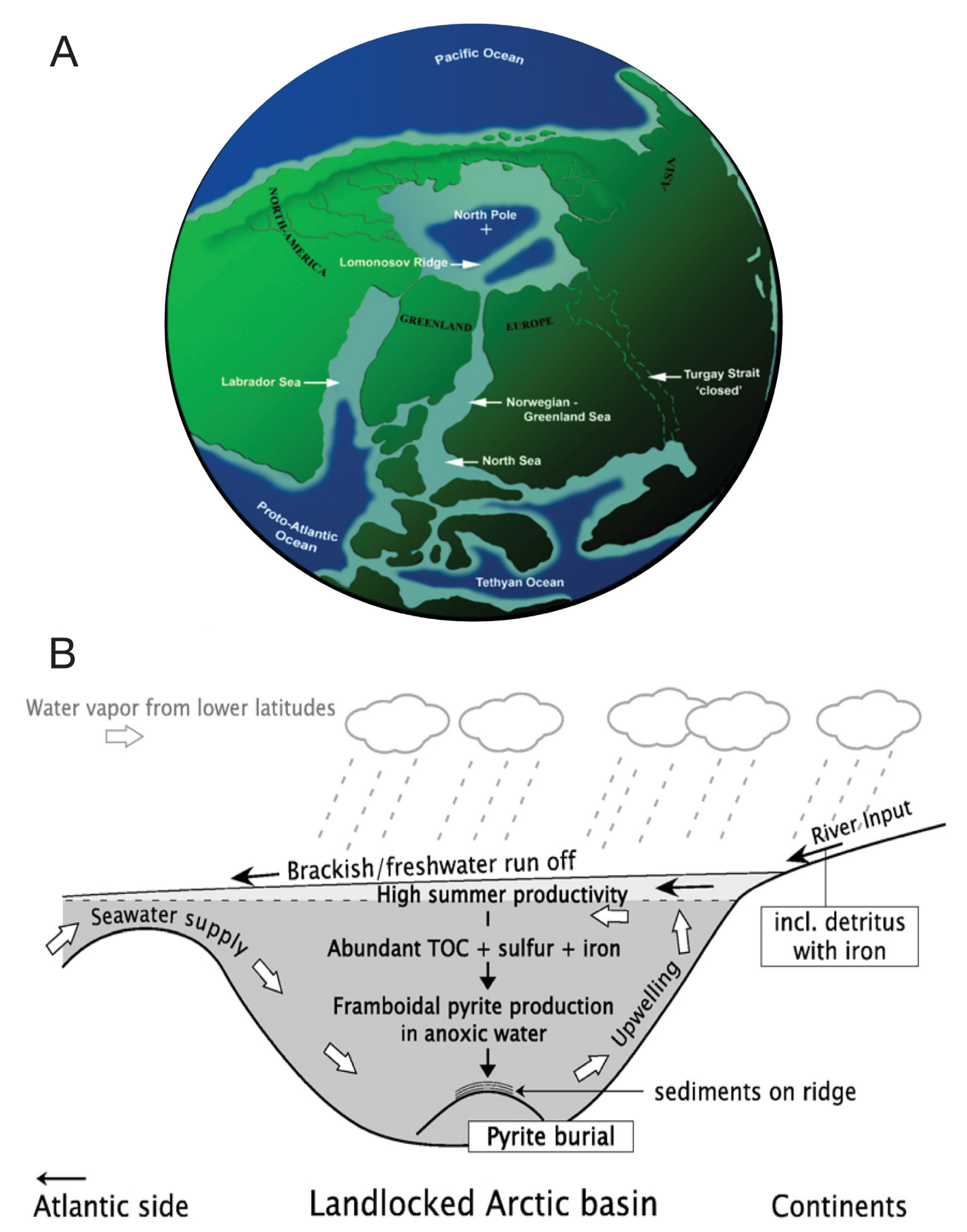


Fig. 5. Reconstruction of the early-middle Eocene Arctic Ocean. (A) Paleogeography of the Arctic region between ~50 and 45 Ma (after Stickley et al., 2009). (B) Illustration of the estuarine circulation pattern and pyrite formation under euxinic conditions in the Eocene Arctic basin (after Ogawa et al., 2008).

2019 and references therein). Second, the intensive evaporite dissolution can drastically increase the availability of sulfate – which is required for MSR as well as AOM – in the ocean (from ~8 mM to over 28 mM; Wortmann and Paytan, 2012). Assuming there is sufficient OM and reactive iron in marine sediments, seawater sulfate concentrations may become the dominant parameter controlling pyrite burial rates in a non-linear way (from ~7  $\times$   $10^{11}$  to ~1  $\times$   $10^{12}$  mol/yr; Wortmann and Chernyavsky, 2007). Although the timing of the India-Eurasia collision is uncertain, the result is still consistent with the refined  $\delta^{34}S_{sw}$  curve by lowering the flux estimate for a more extended period (Yao et al., 2020).

#### 4.5. Sulfur injections from Large Igneous Provinces (LIPs)

Unlike studies that presume a pulse event with no change to the background equilibrium state of the sulfur cycle, Laakso et al. (2020) hypothesize a slow decrease in the burial efficiency of total sulfur dominated by a reduction in absolute sulfide deposition over the past 120 million years. This will lead to a gradual increase in the sulfate-tosulfide burial ratio and seawater sulfate concentration (from 5 mM in the late Cretaceous to > 26 mM today), driving a parallel gradual increase in  $\delta^{34}S_{sw}.$  The superimposed perturbations of the  $\delta^{34}S_{sw}$  signal are then satisfied by large pulses of sulfur (on the scale of  $1 \times 10^{18}$  mol sulfur on million-year timescales) injected to the Earth's surface from the eruption and emplacement of large igneous provinces (LIPs). The isotopically depleted sulfur input from LIPs can transiently lower  $\delta^{34}S_{sw}$ and subsequently increase sulfate concentrations and pyrite burial rates (Paytan et al., 1998; Laakso et al., 2020). Most notably, the emplacement of the North Atlantic Igneous Province and explosive circum-Caribbean volcanism between 63 and 50 Ma (Rea et al., 1990; Eldholm and Thomas, 1993; Bralower et al., 1997; Schmitz et al., 2004; Svensen et al., 2004; Storey et al., 2007; Svensen et al., 2010) coincide with the 2‰ decline and the following 5‰ rise in  $\delta^{34}S_{sw}$  in the early Cenozoic (Fig. 2). In the early-Eocene ocean with a sulfate concentration of ~15 mM, mass balance calculations capture the observed  $\delta^{34}S_{sw}$  signal by forcing volcanic input of  $1.06\times10^{19}$  mol sulfur into the ocean, with the influx culminating at  $\sim 1.7\times10^{12}$  mol S/yr around 55 Ma. Similar processes apply to the sulfur cycle from the late Cretaceous to present (Laakso et al., 2020), such as the gradual  $\delta^{34}S_{sw}$  decrease by 1% since the mid-Miocene is partially due to the increase in sulfur input  $(6.6 \times 10^{18} \, \text{mol})$  from Columbia River Flood Basalt volcanism (Hooper et al., 2002; Self et al., 2006). Although the assumption of a long-term change in the background equilibrium state of sulfate is under debate, the role of SO<sub>2</sub> outgassing during LIPs emplacements indeed provides a possible explanation to the complex  $\delta^{34}S_{sw}$ .

The LIPs-derived perturbations to the global sulfur cycle can be quantitatively assessed through the analysis of the triple oxygen isotope ( $^{17}$ O) in sulfate. Sulfate oxygen derived from atmospheric  $O_2$  via oxidative weathering of pyrite carries a strong negative mass-independent  $^{17}$ O anomaly, while the tropospheric oxidation of outgassed  $SO_2$  can pick up a large positive  $^{17}$ O anomaly (Waldeck et al., 2019). Integrating this novel, emerging isotope system in the context of the global biogeochemical sulfur cycle can further provide an opportunity to constrain weathering, volcanism, pyrite burial, sulfur concentration, and isotope fractionation through time, as well as aid to predict the past atmospheric  $pO_2/pCO_2$  ratio.

### 4.6. Alternative possible triggers and further work

While the above scenarios are all plausible to explain the early-Eocene  $\delta^{34}S_{sw}$  excursion, the question of what changes in the sulfur cycle actually occurred remains open because the system is underconstrained. A recent study based on macrostratigraphic data describes a sulfur cycle in which pyrite weathering and burial fluxes are less variable on a long timescale and are more important than previously thought (Halevy et al., 2012). As such, a large increase in the fraction of

sulfur removed from the ocean by pyrite burial,  $f_{pyrite} = F_{pyrite}$ (F<sub>evaporite</sub> + F<sub>pyrite</sub>), may be associated with low evaporite burial rates rather than high pyrite burial. Notably, evaporate burial is more sporadic and primarily governed by the episodic availability of marine environments suitable for evaporite formation and preservation. The estimated decrease in evaporite precipitation in the early Eocene (Hay et al., 2006; Halevy et al., 2012) is in line with a loss of the area of shallow seas in response to the sea-level decline (Miller et al., 2005). Although a decrease in evaporite burial itself does not directly alter  $\delta^{34}S_{sw}$ , it may result in a subsequent increase in sulfate concentrations (assuming constant sulfur influxes) and thereby pyrite burial rates. In contrast to a sulfide-dominated sulfur cycle (Halevy et al., 2012), Canfield (2013) propose a sulfate-dominated sulfur cycle as constrained by coal S-isotope data. Regardless of different interpretations of the operation of sulfur cycling in a longer timeframe, both model predictions reach the expected agreement on an increase in the fractional pyrite burial flux (i.e.,  $f_{pyrite}$ ) in the early Eocene.

It is noteworthy that in a steady-state sulfur cycle model, a lower f<sub>pvrite</sub> is required to compensate for a larger contribution from evaporite weathering and that an overestimate of riverine sulfate  $\delta^{34}S$  composition will artificially bias the sulfur cycle towards a lower f<sub>pyrite</sub> (Halevy et al., 2012; Tostevin et al., 2014). Indeed, Burke et al. (2018) question the validity of assuming a constant  $\delta^{34}S$  of riverine input to the ocean through time and suggest that secular variations in basin lithologies exposed to weathering can exert a strong control on riverine  $\delta^{34}S$  values, in turn driving  $\delta^{34}S_{sw}$  changes. Some of the scenarios above (e.g., Wortmann and Paytan, 2012; Laakso et al., 2020) also indicate that the 5‰ rise in  $\delta^{34}S_{sw}$  in the early-middle Eocene can be a result of combined effects of changes in the inputs (fluxes and their isotopic values) and changes in pyrite burial rates. As these changes are expected to be large, it is necessary to reassess the relative contributions from weathering of evaporite (associated with the basin-scale evaporite dissolution events), volcanic sulfur (from LIPs) and sedimentary pyrite, and the resulting riverine  $\delta^{34}$ S composition. Complications of ancient sulfur-bearing mineral deposits may provide direct evidence (e.g., distributions of sulfate/sulfide minerals on the continents, weathering rates, volcanisms) to constrain sulfur fluxes and their isotopic values (e.g., Hay et al., 2006; Halevy et al., 2012; Canfield, 2013). With the advancement of multiple S-isotope analyses, investigation of the relationship between  $\delta^{34}S_{sw}$  and  $\delta^{33}S_{sw}$  can also improve estimates of the global pyrite burial flux (Tostevin et al., 2014) and the understanding of the processes involved in the global sulfur cycle. In addition, given the large range of estimates of the difference between seawater sulfate and sedimentary pyrite (i.e.,  $\Delta$ ), more work constraining global variations in  $\Delta$  from modern marine sediments (on continental shelves, slopes, rises, and abyssal environments) will help to resolve this issue.

## 5. Summary

Significant climatic and tectonic perturbations over the Cenozoic may have influenced the global sulfur cycle that is intricately linked to the cycling of carbon, iron, and nutrients. In response to changes in the redox state and biogeochemical processes on the Earth's surface, the  $\delta^{34}S_{sw}$  oscillates through time. Compilation of marine pelagic barite and carbonate associated sulfate data from worldwide deep-sea sediments provides precise information of secular fluctuations in  $\delta^{34}S_{sw}$  for the Cenozoic. This record with much improved biostratigraphy confirms the positive 5% shift in the early-middle Eocene at a rate of approximately 0.4%/Myr. Several scenarios have been proposed to explain the 5% rise in  $\delta^{34}S_{sw}$  between ~55 and 40 Ma. Many of these scenarios are plausible because the parameters defining  $\delta^{34}S_{sw}$  are not well constrained for past geological time. However, while the trigger mechanisms vary, current understanding suggests that changes in pyrite burial in the early Eocene, through changing the burial flux and/or the Sisotope composition of pyrite, are involved (although other changes are not necessarily excluded). The former requires a shift in the dominant

locus of pyrite burial towards a deep ocean setting in response to a rapid sea-level drop, while the latter calls for changes in the average global S-isotope fractionation between seawater sulfate and pyrite through yet unknown controls. Changes in pyrite burial rates globally or locally in the euxinic Eocene Arctic basin and/or input of large pulses of sulfur from basin-scale evaporite dissolution events or Large Igneous Provinces can satisfy the observed increases in  $\delta^{34} S_{\rm sw}$ .

Additional information from different mass-dependent and mass-independent isotopic systematics (e.g.,  $^{33}\text{S}, ^{36}\text{S}, ^{18}\text{O}, ^{17}\text{O})$ , better assessment of the amount and distribution of pyrite burial, and additional constraints on other potential variables (e.g., changes in input fluxes or their isotopic signatures) may provide new insights into the evolution of microbial ecology and the reconstruction of the global sulfur cycle. Although this study targets the story of sulfur in seawater for the Cenozoic, similar models are applicable where perturbations of  $\delta^{34}\text{S}_{sw}$  are seen throughout Earth history. High precision  $\delta^{34}\text{S}_{sw}$  records can further be utilized for stratigraphic correlations, especially during times of rapid perturbations (e.g., Yao et al., 2019).

#### Declaration of competing interest

We wish to confirm that there are no known conflicts of interest associated with this publication and there has been no significant financial support for this work that could have influenced its outcome.

#### Acknowledgments

This work was supported the National Science Foundation (NSF) CAREER grant (OCE-0449732) and OCE-1827431 to A.P.

#### Appendix A. Supplementary data

Supplementary data to this article can be found online at https://doi.org/10.1016/j.chemgeo.2020.119788.

#### References

- Akhmetiev, M.A., Beniamovski, V.N., 2004. Paleocene and Eocene of Western Eurasia (Russian sector) — stratigraphy, palaeogeography, climate. N. Jb. Geol. Paläont. (Abh.) 234, 137–181.
- Antler, G., Turchyn, A.V., Rennie, V., Herut, B., Sivan, O., 2013. Coupled sulfur and oxygen isotope insight into bacterial sulfate reduction in the natural environment. Geochim. Cosmochim. Acta 118, 98–117.
- Antler, G., Turchyn, A.V., Ono, S., Sivan, O., Bosak, T., 2017. Combined <sup>34</sup>S, <sup>33</sup>S and <sup>18</sup>O isotope fractionations record different intracellular steps of microbial sulfate reduction. Geochim. Cosmochim. Acta 203, 364–380.
- Balci, N., Mayer, B., Shanks, W.C., Mandernack, K.W., 2012. Oxygen and sulfur isotope systematics of sulfate produced during abiotic and bacterial oxidation of sphalerite and elemental sulfur. Geochim. Cosmochim. Acta 77, 335–351.
- Berger, W.H., 1970. Biogenous deep-sea sediments: fractionation by deep-sea circulation. Geol. Soc. Am. Bull. 81, 1385–1402.
- Berner, R.A., 1970. Sedimentary pyrite formation. Am. J. Sci. 268, 1-23.
- Berner, R.A., 1982. Burial of organic-carbon and pyrite sulfur in the modern ocean its geochemical and environmental significance. Am. J. Sci. 282, 451–473.
- Berner, R.A., 1989. Biogeochemical cycles of carbon and sulfur and their effect on atmospheric oxygen over phanerozoic time. Palaeogeogr. Palaeoclimatol. Palaeoecol. 75, 97–112.
- Berner, E.K., Berner, R.A., 1987. The Global Water Cycle Geochemistry and Environment. Prentice-Hall, New Jersey (397 p).
- Berner, R.A., Raiswell, R., 1983. Burial of organic carbon and pyrite sulfur in sediments over Phanerozoic time: a new theory. Geochim. Cosmochim. Acta 47, 855–862.
- Böttcher, M.E., Thamdrup, B., 2001. Anaerobic sulfide oxidation and stable isotope fractionation associated with bacterial sulfur disproportionation in the presence of MnO<sub>2</sub>. Geochim. Cosmochim. Acta 65, 1573–1581.
- Böttcher, M.E., Thamdrup, B., Vennemann, T.W., 2001. Oxygen and sulfur isotope fractionation during anaerobic bacterial disproportionation of elemental sulfur. Geochim. Cosmochim. Acta 65, 1601–1609.
- Böttcher, M.E., Rinna, J., Warning, B., Wehausen, R., Howell, M.W., Schnetger, B., Stein, R., Brumsack, H.J., Rullkötter, J., 2003. Geochemistry of sediments from the connection between the western and the eastern Mediterranean Sea (Strait of Sicily, ODP Site 963). Palaeogeogr. Palaeoclimatol. Palaeoecol. 190, 165–194.

  Böttcher, M.E., Thamdrup, B., Gehre, M., Theune, A., 2005. <sup>34</sup>S/<sup>32</sup>S and <sup>18</sup>O/<sup>16</sup>O frac-
- Böttcher, M.E., Thamdrup, B., Gehre, M., Theune, A., 2005. 34S/32S and 18O/16O fractionation during sulfur disproportionation by Desulfobulbus propionicus. Geomicrobiol J. 22, 219–226.

Bottrell, S.H., Newton, R.J., 2006. Reconstruction of changes in global sulfur cycling from marine sulfate isotopes. Earth Sci. Rev. 75, 59–83.

- Bouilhol, P., Jagoutz, O., Hanchar, J.M., Dudas, F.O., 2013. Dating the India– Eurasia collision through arc magmatic records. Earth Planet. Sci. Lett. 366, 163–175.
- Bralower, T.J., Thomas, D.J., Zachos, J.C., Hirschmann, M., Röhl, U., Sigurdsson, H., Thomas, E., Whitney, D., 1997. High-resolution records of the Late Paleocene Thermal Maximum and Caribbean volcanism: is there a causal link? Geology 25, 963–965.
- Brumsack, H.J., 1980. Geochemistry of Cretaceous black shales from the Atlantic Ocean (DSDP Legs 11, 14, 36 and 41). Chem. Geol. 31, 1–25.
- Brunner, B., Bernasconi, S.M., 2005. A revised isotope fractionation model fordissimilatory sulfate reduction in sulfate reducing bacteria. Geochim. Cosmochim. Acta 69, 4759–4771.
- Burke, A., Present, T.M., Paris, G., Rae, E.C.M., Sandilands, B.H., Gaillardet, J., Peucker-Ehrenbrink, B., Fischer, W.W., McClelland, J.W., Spencer, R.G.M., Voss, B.M., Adkins, J.F., 2018. Sulfur isotopes in rivers: insights into global weathering budgets, pyrite oxidation, and the modern sulfur cycle. Earth Planet. Sci. Lett. 496, 168–177.
- Calmels, D., Gaillardet, J., Brenot, A., France-Lanord, C., 2007. Sustained sulfide oxidation by physical erosion processes in the Mackenzie River basin: climatic perspectives. Geology 35, 1003–1006.
- Canfield, D.E., 2004. The evolution of the Earth surface sulfur reservoir. Am. J. Sci. 304, 839–861.
- Canfield, D.E., 2013. Sulfur isotopes in coal constrain the evolution of the Phanerozoic sulfur cycle. Proceedings of the National Academy of Science USA 110, 8443–8446.
- Canfield, D.E., Farquhar, J., Zerkle, A.L., 2010. High isotope fractionations during sulfate reduction in a low-sulfate euxinic ocean analog. Geology 38, 415–418.
- Claypool, G.E., Holser, W.T., Kaplan, I.R., Sakai, H., Zak, I., 1980. The age curves of sulfur and oxygen isotopes in marine sulfate and their mutual interpretation. Chem. Geol. 28, 199–260.
- Cleveland, W.S., 1979. Robust locally weighted regression and smoothing scatterplots. J. Am. Stat. Assoc. 74, 829–836.
- Coplen, T.B., Hopple, J.A., Böhlke, J.K., et al., 2001. Compilation of minimum and maximum isotope ratios of selected elements in naturally occurring terrestrial materials and reagents. In: U.S. Geological Survey Water-Resources Investigations Report, (4222 p).
- Dervos, C.T., Vassiliou, P., 2000. Sulfur hexafluoride (SF<sub>6</sub>): global environmental effects and toxic byproduct formation. J. Air Waste Manage. Assoc. 50, 137–141.
- Dickson, A.J., Cohen, A.S., 2012. A molybdenum isotope record of Eocene Thermal Maximum 2: implications for global ocean redox during the early Eocene. Paleoceanography 27 (PA3230).
- Dymond, J., Suess, E., Lyle, M., 1992. Barium in deep-sea sediments. A geochemical proxy for paleoproductivity. Paleoceanography 7, 163–181.
- Eldholm, O., Thomas, E., 1993. Environmental impact of volcanic margin formation. Earth Planet. Sci. Lett. 117, 319–329.
- Farquhar, J., Wing, B.A., 2003. Multiple sulfur isotopes and the evolution of the atmosphere. Earth Planet. Sci. Lett. 213, 1–13.
- Fike, D.A., Bradley, A.S., Rose, C.V., 2015. Rethinking the ancient sulfur cycle. Annu. Rev. Earth Planet. Sci. 43, 593–622.
- Froelich, P.N., Klinkhammer, G.P., Bender, M.L., Luedtke, N.A., Heath, G.R., Cullen, D., Dauphin, P., Hammond, D., Hartman, B., Maynard, V., 1979. Early oxidation of organic matter in pelagic sediments of the eastern equatorial Atlantic: suboxic diagenesis. Geochim. Cosmochim. Acta 43, 1075–1090.
- Gao, X., Thiemens, M.H., 1993. Isotopic composition and concentration of sulfur in carbonaceous chondrites. Geochim. Cosmochim. Acta 57, 3159–3169.
- Garrels, R.M., Lerman, A., 1984. Coupling of the sedimentary sulfur and carbon cycles an improved model. Am. J. Sci. 284, 989–1007.
- Goldhaber, M.B., Kaplan, I.R., 1975. Controls and consequences of sulfate reduction rates in recent marine sediments. Soil Sci. 119, 42–55.
- Golonka, J., 2004. Plate tectonic evolution of the southern margin of Eurasia in the Mesozoic and Cenozoic. Tectonophysics 381, 235–273.
- Gradstein, F.M., Ogg, J.G., Schmitz, M., Ogg, G., 2012. The Geologic Time Scale 2012. (1176 p).
- Grassineau, N.V., Mattey, D.P., Lowry, D., 2001. Sulfur isotope analysis of sulfide and sulfate minerals by continuous flow-isotope ratio mass spectrometry. Anal. Chem. 73, 220–225.
- Halevy, I., Peters, S.E., Fischer, W.W., 2012. Sulfate burial constraints on the Phanerozoic sulfur cycle. Science 337, 331–334.
- Hansen, K.W., Wallman, K., 2003. Cretaceous and Cenozoic evolution of seawater composition, atmospheric O<sub>2</sub> and CO<sub>2</sub> a model perspective. Am. J. Sci. 303, 94–148.
- Hay, W.W., Migdisov, A., Balukhovsky, A.N., Wold, C.N., Flögel, S., Söding, E., 2006. Evaporites and the salinity of the ocean during the Phanerozoic: implications for climate, ocean circulation and life. Palaeogeogr. Palaeoclimatol. Palaeoecol. 240, 3–46.
- Holland, H.D., 1974. Marine evaporites and the composition of sea water during the Phanerozoic. Society of Economic Paleontologists and Mineralogists Special Paper 20, 187–192.
- Holser, W.T., Schidlowski, M., Mackenzie, F.T., Maynard, J.B., 1988. Biogeochemicla cycles of carbon and sulfur. In: Gregor, C.B., Garrels, R.M., Mackenzie, F.T., Maynard, J.B. (Eds.), Chemical Cycles in the Evolution of the Earth. John Wiley and Sons, New York, pp. 105–173.
- Hooper, P.R., Binger, G.B., Lees, K.R., 2002. Ages of the Steens and Columbia River flood basalts and their relationship to extension-related calc-alkalic volcanism in eastern Oregon. Geol. Soc. Am. Bull. 114, 43–50.
- Horita, J., Zimmermann, H., Holland, H.D., 2002. Chemical evolution of seawater during the Phanerozoic: implications from the record of marine evaporites. Geochim. Cosmochim. Acta 66, 3733–3756.

- Hurtgen, M.T., 2012. The marine sulfur cycle, revisited. Science 337, 305-306.
- Johnston, D.T., 2011. Multiple sulfur isotopes and the evolution of Earth's surface sulfur cycle. Earth Sci. Rev. 106, 161–183.
- Johnston, D.T., Farquhar, J., Wing, B.A., Kaufman, A.J., Canfield, D.E., Habicht, K.S., 2005. Multiple sulfur isotope fractionations in biological systems: a case study with sulfate reducers and sulfur disproportionators. Am. J. Sci. 305, 645–660.
- Johnston, D.T., Farquhar, J., Habicht, K.S., Canfield, D.E., 2008. Sulphur isotopes and the search for life: strategies for identifying sulphur metabolisms in the rock record and beyond. Geobiology 6, 425–435.
- Jørgensen, B.B., 1982. Mineralization of organic-matter in the sea bed the role of sulfate reduction. Nature 296, 643–645.
- Jørgensen, B.B., 1987. Ecology of the sulphur cycle: oxidative pathways in sediments. In: Cole, J.A., Ferguson, S. (Eds.), The Nitrogen and Sulphur Cycles. vol. 42. The Society for General Microbiology, pp. 31–36.
- Jørgensen, B.B., Kasten, S., 2006. Sulfur cycling and methane oxidation. In: Schulz, H.D., Zabel, M. (Eds.), Marine Geochemistry, 2nd edition. Springer, Berlin, pp. 271–309.
- Jørgensen, B.B., Nelson, D.C., 2004. Sulfide oxidation in marine sediments: geochemistry meets microbiology. In: Ahmend, J.P., Edwards, K.J., Lyons, T.W. (Eds.), Sulfur Biogeochemistry - Past and Present. Geological Society of America Special Paper. vol. 379. pp. 63–82.
- Jørgensen, B.B., Fossing, H., Wirsen, C.O., Jannasch, H.W., 1991. Sulfide oxidation in the anoxic Black Sea chemocline. Deep-Sea Res. 38, S1083–S1103.
- Kampschulte, A., Strauss, H., 2004. The sulfur isotopic evolution of Phanerozoic seawater based on the analysis of structurally substituted sulfate in carbonates. Chem. Geol. 204, 255–286.
- Kampschulte, A., Bruckschen, P., Strauss, H., 2001. The sulphur isotopic composition of trace sulphates in Carboniferous brachiopods: implications for coeval seawater, correlation with other geochemical cycles and isotope stratigraphy. Chem. Geol. 175, 149–173
- Kaplan, I.R., Emery, K.O., Rittenberg, S.C., 1963. The distribution and isotopic abundance of sulphur in recent marine sediments off southern California. Geochim. Cosmochim. Acta 27, 297–331.
- Kasten, S., Jorgensen, B.B., 2000. Sulfate reduction in marine sediments. In: Schulz, H.D., Zabel, M. (Eds.), Marine Chemistry, pp. 263–275.
- Kohn, M.J., Riciputi, L.R., Stakes, D., Orange, D.L., 1998. Sulfur isotope variability in biogenic pyrite: reflections of heterogenous bacterial colonization? Am. Mineral. 83, 1454–1468.
- Kölling, M., Bouimetarhan, I., Bowles, M.W., et al., 2019. Consistent CO<sub>2</sub> release by pyrite oxidation on continental shelves prior to glacial terminations. Nat. Geosci. 12, 929–934.
- Kump, L.R., Garrels, R.M., 1986. Modeling atmospheric O<sub>2</sub> in the global sedimentary redox cycle. Am. J. Sci. 286, 337–360.
- Kunzmann, M., Bui, T.H., Crockford, P.W., Halverson, G.P., Scott, C., Lyons, T.W., Wing, B.A., 2017. Bacterial sulfur disproportionation constrains timing of Neoproterozoic oxygenation. Geology 45, 207–210.
- Kurtz, A.C., Kump, L.R., Arthur, M.A., Zachos, J., Paytan, A., 2003. Early Cenozoic decoupling of the global carbon and sulfur cycles. Paleoceanography 18, 1090–1103.
- Laakso, T., Waldeck, A., Macdonals, F., Johnston, D., 2020. Volcanic controls on seawater sulfate over the past 120 million years. PNAS In Press.
- Lazarus, D.B., 1994. Neptune: a marine Micropaleontology Database. Math. Geol. 26, 817–832.
- Lyons, T.W., Berner, R.A., 1992. Carbon–sulfur–iron systematics of the uppermost deepwater sediments of the Black Sea. Chem. Geol. 99, 1–27.
- MacNamara, J., Thode, H.G., 1950. Comparison of the isotopic constitution of terrestrial and meteoritic sulphur. Phys. Rev. 78, 307.
- Markovic, S., Paytan, A., Wortmann, U.G., 2015. Pleistocene sediment offloading and the global sulfur cycle. Biogeosciences 12, 3043–3060.
- Markovic, S., Paytan, A., Li, H., Wortmann, U.G., 2016. A revised seawater sulfate oxygen isotope record for the last 4 Myr. Geochim. Cosmochim. Acta 175, 239–251.
- Masterson, A.L., Wing, B.A., Paytan, A., Farquhar, J., Johnston, D.T., 2016. The minor sulfur isotope composition of Cretaceous and Cenozoic seawater sulfate. Paleoceanography 31, 779–788.
- Meija, J., Coplen, T.B., Berglund, M., Brand, W.A., De Bièvre, P., Gröning, M., Holden, N.E., Irrgeher, J., Loss, R.D., Walczyk, T., Prohaska, T., 2016. Atomic weights of the elements 2013 (IUPAC Technical Report). Pure Appl. Chem. 88, 265–291.
- Meybeck, M., 1979. Concentrations des eaux fluviales en éléments majeurs et apports en solution aux océans. Revue de Geologie Dynamiqe et de Geographie Physique 21, 215–246.
- Meyer, K.M., Kump, L.R., 2008. Oceanic Euxinia in Earth history: causes and Consequences. Annu. Rev. Earth Planet. Sci. 36, 251–288.
- Miller, K.G., Kominz, M.A., Browning, J.V., Wright, J.D., Mountain, G.S., Katz, M.E., Sugarman, P.J., Cramer, B.S., Christie-Blick, N., Pekar, S.F., 2005. The Phanerozoic record of global sea-level change. Science 310, 1293–1298.
- Millero, F.J., 2005. Chemical Oceanography, 3rd edition. CRC Press, Boca Raton, Florida (520 p).
- Moses, C.O., Nordstrom, D.K., Herman, J.S., Mills, A.L., 1987. Aqueous pyrite oxidation by dissolved-oxygen and by ferric iron. Geochim. Cosmochim. Acta 51, 1561–1571.
- Newell, A.J., 2001. Construction of a Paleogene tide dominated shelf: influence of Top Chalk topography and sediment supply (Wessex Basin, UK). J. Geol. Soc. 158, 379–390.
- Ogawa, T., Furusawa, T., Nomura, R., Seo, D., Hosoya-Matsuda, N., Sakurai, H., Inoue, K., 2008. SoxAX binding protein, a novel component of the thiosulfate oxidizing multienzyme system in the green sulfur bacterium Chlorobium tepidum. J. Bacteriol. 190, 6097–6110. https://doi.org/10.1128/JB.00634-08.
- Ogawa, Y., Takahashi, K., Yamanaka, T., Onodera, J., 2009. Significance of euxinic condition in the middle Eocene paleo-Arctic basin: a geochemical study on the IODP

- Arctic coring expedition 302 sediments. Earth Planet. Sci. Lett. 285, 190-197.
- Ohmoto, H., Rye, R.O., 1979. Isotope of sulfur and carbon. In: Barnes, H.L. (Ed.), Geochemistry of Hydrothermal Ore Deposits, 2nd edition. John Wiley and Sons, New York, pp. 509–567.
- Orti, F., Rosell, L., Anadón, P., 2010. Diagenetic gypsum related to sulfur deposits in evaporites (Libros Gypsum, Miocene, NE Spain). Sediment. Geol. 228, 304–318.
- Paris, G., Sessions, A.L., Subhas, A.V., Adkins, J.F., 2013. MC-ICP-MS measurement of  $\delta^{34}$ S and  $\Delta^{33}$ S in small amounts of dissolved sulfate. Chem. Geol. 345, 50–61.
- Paris, G., Fehrenbacher, J.S., Sessions, A.L., Spero, H.J., Adkins, J.F., 2014. Experimental determination of carbonate-associated sulfate  $\delta$ 34S in planktonic foraminifera shells. Geochem. Geophys. Geosyst. 15, 1452–1461.
- Paytan, A., Kastner, M., Campbell, D., Thiemens, M.H., 1998. Sulfur isotopic composition of Cenozoic seawater sulfate. Science 282, 1459–1462.
- Paytan, A., Mearon, S., Cobb, K., Kastner, M., 2002. Origin of marine barite deposits: Sr and S isotope characterization. Geology 30, 747–750.
- Paytan, A., Kastner, M., Campbell, D., Thiemens, M.H., 2004. Seawater sulfur isotope fluctuations in the Cretaceous. Science 304, 1663–1665.
- Petsch, S.T., Berner, R.A., 1998. Coupling the geochemical cycles of C, P, Fe, and S: the effect on atmospheric O<sub>2</sub> and the isotopic records of carbon and sulfur. Am. J. Sci. 298, 246–262.
- R Core Team, 2012. R: A Language and Environment for Statistical Computing. R Foundation for Statistical Computing, Vienna, Austria.
- Raiswell, R., Berner, R.A., 1985. Pyrite formation in euxinic and semi-euxinic sediments. Am. J. Sci. 285, 710–724.
- Rea, D.K., Zachos, J.C., Owen, R.M., Gingerich, P.D., 1990. Global change at the Paleocene-Eocene boundary: climatic and evolutionary consequences of tectonic events. Paleogeography, Paleoclimatology, Paleoecology 79, 117–128.
- Reeburgh, W.S., 1983. Rates of biogeochemical processes in anoxic sediments. Annu. Rev. Earth Planet. Sci. 11, 269–298.
- Rees, C.E., Jenkins, W.H., Monster, J., 1978. Sulfur isotopic composition of ocean water sulfate. Geochim. Cosmochim. Acta 42, 377–381.
- Rennie, V.C.F., Turchyn, A.V., 2014. The preservation of  $\delta^{34}S_{SO4}$  and  $\delta^{18}O_{SO4}$  in carbonate-associated sulfate during marine diagenesis. A 25 Myr test case using marine sediments. Earth Planet. Sci. Lett. 395, 13–23.
- Rennie, V.C.F., Paris, G., Sessions, A.L., Abramovich, A., Turchyn, A.V., Adkins, J.F., 2018. Cenozoic record of  $\delta^{34}$ S in foraminiferal calcite implies an early Eocene shift to deep-ocean sulfide burial. Nat. Geosci. 11, 761–765.
- Rickard, D., 2012. Sulfidic Sediments and Sedimentary Rocks. Elsevier Academic Press, Amsterdam (816 p).
- Ross, P.S., Peateb, I. Ukstins, McClintocka, M.K., Xuc, Y.G., Skillingd, I.P., Whitea, J.D.L., Houghtone, B.F., 2005. Mafic volcaniclastic deposits in flood basalt provinces: a review. J. Volcanol. Geotherm. Res. 145, 281–314.
- Rudnicki, M.D., Elderfield, H., Spiro, B., 2001. Fractionation of sulfur isotopes during bacterial sulfate reduction in deep ocean sediments at elevated temperatures. Geochim. Cosmochim. Acta 65, 777–789.
- Sakai, H., Casadevall, T.J., Moore, J.G., 1982. Chemistry and isotope ratios of sulfur in basalts and volcanic gases at Kilauea Volcano, Hawaii. Geochim. Cosmochim. Acta 46, 729–738
- Schmitz, B., Peucker-Ehrenbrink, B., Heilmann-Clausen, C., Aberg, G., Asaro, F., Lee, C.T., 2004. Basaltic explosive volcanism, but no comet impact at the Paleocene-Eocene boundary: High resolution chemical and isotope records from Egypt, Spain and Denmark. Earth Planet. Sci. Lett. 225, 1–17.
- Self, S., Widdowson, M., Thordarson, T., Jay, A.E., 2006. Volatile fluxes during flood basalt eruptions and potential effects on the global environment: a Deccan perspective. Earth Planet. Sci. Lett. 248, 517–531.
- Sim, M.S., Bosak, T., Ono, S., 2011. Large sulfur isotope fractionation does not require disproportionation. Science 333, 74–77.
- Spencer-Cervato, C., 1999. The Cenozoic Deep Sea Microfossil Record: Explorations of the DSDP/ODP Sample Set Using the Neptune Database. (270 p).
- Stein, R., Boucsein, B., Meyer, H., 2006. Anoxia and high primary production in the Paleogene Central Arctic Ocean: first detailed records from Lomonosov Ridge. Geophys. Res. Lett. 33, L18606.
- Stickley, C.E., John, K.S., Koç, N., Jordan, R.W., Passchier, S., Pearce, R.B., Kearns, L.E., 2009. Evidence for middle Eocene Arctic Sea ice from diatoms and ice-rafted debris. Nature 460, 376–379.
- Stoiber, R.E., Williams, S.N., Huebert, B., 1987. Annual contribution of sulfur dioxide to the atmosphere by volcanoes. J. Volcanol. Geotherm. Res. 33, 1–88.
- Storey, M., Duncan, R.A., Swisher, C.C., 2007. Paleocene-Eocene thermal Maximum and the opening of the Northeast Atlantic. Science 316, 587–589.
- Strauss, H., 1997. The isotopic composition of sedimentary sulfur through time. Paleogeography, Paleoclimatology, Paleoecology 132, 97–118.
- Strauss, H., Banerjee, D.M., Kumar, V., 2001. The sulfur isotopic composition of Neoproterozoic to early Cambrian seawater—evidence from the cyclic Hanseran evaporites, NW India. Chem. Geol. 175, 17–28.
- Svensen, H., Planke, S., Malthe-Sørenssen, A., Jamtveit, B., Myklebust, R., Eidem, T.R., Rey, S.S., 2004. Release of methane from a volcanic basin as a mechanism for initial Eocene global warming. Nature 429, 542–545.
- Svensen, H., Planke, S., Corfu, F., 2010. Zircon dating ties NE Atlantic sill emplacement to initial Eocene global warming. J. Geol. Soc. 167, 433–436.
- Thamdrup, B., Fossing, H., Jrgensen, B.B., 1994. Manganese, iron, and sulfur cycling in a coastal marine sediment, Aarhus Bay, Denmark. Geochim. Cosmochim. Acta 58, 5115–5129.
- Torres, M.E., Brumsack, H.J., Bohrmann, G., Emeis, K.C., 1996. Barite fronts in continental sediments: a new look at barium remobilization in the zone of sulfate reduction and formation of heavy barites in authigenic fronts. Chem. Geol. 127, 125–139.

Tostevin, R., Turchyn, A.V., Farquhar, J., Johnston, D.T., Eldridge, D.L., Bishop, J.K.B., McIlvin, M., 2014. Multiple sulfur isotope constraints on the modern sulfur cycle. Earth Planet. Sci. Lett. 396, 14–21.

- Toyama, K., Paytan, A., Sawada, K., Hasegaw, T., 2020. Sulfur isotope ratios in co-occurring barite and carbonate from Eocene sediments: a comparison study. Chem. Geol. 535, 119454.
- Turchyn, A.V., Schrag, D.P., 2006. Cenozoic evolution of the sulfur cycle: insight from oxygen isotopes in marine sulfate. Earth Planet. Sci. Lett. 241, 763–779.
- Turchyn, A.V., Schrag, D.P., Coccioni, R., Montanari, A., 2009. Stable isotope analysis of the Cretaceous sulfur cycle. Earth Planet. Sci. Lett. 285, 115–123.
- Utrilla, R., Pierre, C., Orti, F., Pueyo, J.J., 1992. Oxygen and sulphur isotope compositions as indicators of the origin of Mesozoic and Cenozoic evaporites from Spain. Chem. Geol. 102, 229–244.
- Valentine, D.L., 2002. Biogeochemistry and microbial ecology of methane oxidation in anoxic environments: a review. Antonie Van Leeuwenhoek 81, 271–282.
- Van Stempvoort, D.R., Krouse, H.R., 1994. Controls of  $\delta^{18}$ O in sulfate review of experimental data and application to specific environments. In: Alpers, C.N., Blowes, D.W. (Eds.), Environmental Geochemistry of Sulfide Oxidation. vol. 550. American Chemical Society, Washington, D.C, pp. 446–480.
- Waldeck, A., Bertran, E., Halevy, I., Wing, B., Johnston, D., 2019. Deciphering the atmospheric signal in marine sulfate oxygen isotope composition. Earth Planet. Sci. Lett. 522, 12–19.
- Walker, J.C.G., 1986. Global geochemical cycles of carbon, sulfur, and oxygen. Mar. Geol. 70, 159–174.
- Wing, B.A., Halevy, I., 2014. Intracellular metabolite levels shape sulfur isotope fractionation during microbial sulfate respiration. Proceedings of the National Academy of Science USA 111, 18116–18125.
- Wortmann, U.G., Chernyavsky, B.M., 2007. Effect of evaporite deposition on Early Cretaceous carbon and sulphur cycling. Nature 446, 654–656.
- Wortmann, U.G., Paytan, A., 2012. Rapid variability of seawater chemistry over the past 130 million years. Science 337, 334–336.

Wortmann, U.G., Bernasconi, S.M., Böttcher, M.E., 2001. Hypersulfidic deep biosphere indicates extreme sulfur isotope fractionation during single-step microbial sulfate reduction. Geology 29, 647–650.

- Wu, N., Farquhar, J., Strauss, H., Kim, S.T., Canfield, D.E., 2010. Evaluating the S-isotope fractionation associated with Phanerozoic pyrite burial. Geochim. Cosmochim. Acta 74, 2053–2071.
- Wu, Nanping, Farquhar, James, Fike, David A., 2015. Ediacaran sulfur cycle: Insights from sulfur isotope measurements ( $\Delta 33S$  and  $\delta 34S$ ) on paired sulfate–pyrite in the Huqf Supergroup of Oman. Geochim. Cosmochim. Acta (0016-7037) 164, 352–364. https://doi.org/10.1016/j.gca.2015.05.031.
- Yao, W., Paytan, A., Wortmann, U.G., 2018. Large-scale ocean deoxygenation during the Paleocene-Eocene Thermal Maximum. Science 361, 804–806.
- Yao, W., Wortmann, U.G., Paytan, A., 2019. Sulfur isotope use for stratigraphy during times of rapid perturbations. In: Montenari, M. (Ed.), Stratigraphy and Timescales. vol. Volume 4. Elsevier Academic Press, Amsterdam, pp. 1–33.
- Yao W., Paytan A., Griffith E.M., Martínez-Ruiz F., Markovic S., and Wortmann U.G., 2020. A revised seawater sulfate S-isotope curve for the Eocene. Chem. Geol. 532, 119382.
- Zachos, J.C., Pagani, M., Sloan, L., Thomas, E., Billups, K., 2001. Trends, rhythms, and aberrations in global climate 65 Ma to present. Science 292, 686–693.
- Zerkle, A.L., Farquhar, J., Johnston, D.T., Cox, R.P., Canfield, D.E., 2009. Fractionation of multiple sulfur isotopes during phototrophic oxidation of sulfide and elemental sulfur by a green sulfur bacterium. Geochim. Cosmochim. Acta 73, 291–306.
- Zerkle, A.L., Kamyshny, A., Kump, L.R., Farquhar, J., Oduro, H., Arthur, M.A., 2010.
  Sulfur cycling in a stratified euxinic lake with moderately high sulfate: constraints from quadruple S isotopes. Geochim. Cosmochim. Acta 74, 4953–4970.
- Zharkov, M.A., 1981. History of Paleozoic Salt Accumulation. Springer-Verlag, Berlin (308 p).
- Zopfi, J., Ferdelman, T.G., Jørgensen, B.B., Teske, A., Thamdrup, B., 2001. Influence of water column dynamics on sulfide oxidation and other major biogeochemical processes in the chemocline of Mariager Fjord (Denmark). Mar. Chem. 74, 29–51.